JOURNAL OF CATALYSIS 137, 139–157 (1992)

Oxidation of Carbon Monoxide over Palladium on Zirconia Prepared from Amorphous Pd–Zr Alloy

II. The Nature of the Active Surface

R. SCHLÖGL,[1,*] G. LOOSE,* M. WESEMANN,* AND A. BAIKER†

*Fritz Haber Institut der Max-Planck Gesellschaft, Faradayweg 4, W 1000 Berlin 33, Germany; and
†Department of Industrial and Engineering Chemistry, Swiss Federal Institute of Technology, ETH Zentrum, CH-8092 Zurich, Switzerland

Received October 29, 1991; revised February 29, 1992

The oxidation of dilute mixtures of CO with dilute oxygen to CO_2 procedes efficiently at moderate temperatures over a catalyst prepared from *in-situ* activation of amorphous $PdZr_2$ alloys. The process of activation and the nature of the activated surface are investigated by XPS, UPS, and low pressure reaction experiments. It turned out to be crucial to perform the activation *"in situ"* in a special reaction chamber. The simultaneous presence of oxidizing and reducing components in the gas leads to the formation of particles of a solid solution of oxygen in Pd (Pd + O) in intimate contact to an ion conducting phase of zirconia. The interface between the two types of particles is large and influences the chemical stability of the Pd + O. It is preformed in the rapid solidification process which leads to a disc-shaped morphology of the micrograins in the alloy. The arrangement is capable of storing chemically active oxygen. The superior catalytic performance of this system relative to a conventional impregnated Pd/ZrO_2 catalyst is traced back to the intimate contact of the oxygen storage phase, zirconia, with the active phase, Pd + O, which is stabilized against reduction to the pure metal by a constant supply of oxygen ions through the bulk of the supporting matrix and the surface of the particle. © 1992 Academic Press, Inc.

1. INTRODUCTION

Purification of gases contaminated by small partial pressures of CO is achieved by CO oxidation over supported noble metal catalysts. Recently the application of amorphous $PdZr_2$ alloys as precursor for a highly active oxidation catalyst has been described (*1, 2*). The turnover frequency of the novel material was found to be an order of magnitude superior to impregnated Pd/ZrO_2 reference catalysts (*2*).

The structural and chemical properties of the new catalyst were studied by several bulk sensitive techniques including TG, DTA, XRD, SEM, and HRTEM. The results suggested a different structure of the new catalyst as compared to the spherical particles of Pd metal supported on stoichiometric zirconia. It was concluded that the catalysts derived from the amorphous Pd_1Zr_2 are made up of small, intergrown, and poorly crystalline domains of different palladium and zirconia phases. Palladium is mainly present as a solid solution with oxygen (Pd + O), whereas zirconia exists in monoclinic and tetragonal forms. The resulting large interface and the ion conducting properties of zirconia for oxide anions were thought to provide the reaction centers located on the Pd particles with a high internal partial pressure of oxide anions. Oxygen thus has not only to be chemisorbed on Pd in order to react with CO, it can also be

[1] To whom correspondence should be addressed: Institut für Anorganische Chemie, Universität Frankfurt, Niederurseler Hang, D-6000 Frankfurt 50.

0021-9517/92 $5.00
Copyright © 1992 by Academic Press, Inc.
All rights of reproduction in any form reserved.

transported from the dominating support surface to the reaction center.

In this picture the characterization and chemical properties of an intermediate compound between Pd metal and PdO plays a central role. This Pd + O solid solution phase occurs in the process of interaction of oxygen with metallic Pd (*3*) and was experimentally obtained by thermal decomposition of various PdO samples (*4, 5*). In these reference experiments spectroscopic properties are described which can be used as fingerprints for Pd + O, which was for the first time characterized by a bulk lattice expansion in (*2*).

The properties of zirconia as ion conductor and its dependence on nonstoichiometry are well established and have been reviewed in (*6*). It is pointed out that the generation of defined zirconia requires usually high-temperature treatments significantly higher than the reaction temperatures applied here. The high temperatures are needed to overcome the barriers, e.g., solid-state annealing processes, which are greatly facilitated in the present case where a metastable Zr alloy precursor is used. This is underlined by the fact that a metastable high-temperature form of zirconia coexists in the activated catalyst with the usual zirconia modification.

The aim of this work is to investigate the surface chemical processes associated with the catalyst activation and to identify the chemical nature of the active surface. In this way the relevance of the bulk structural model suggested in (*2*) for the surface catalytic activity is investigated. It is pointed out that it was found essential to activate the catalysts under atmospheric pressure and practical temperatures "*in-situ*," i.e., in a reaction chamber attached to the electron spectrometer as the catalyst surfaces are highly unstable in air. In preliminary experiments it was further found that the composition of the gas phase is of crucial importance for the surface composition of the activated catalyst, which can vary from entirely oxidic to strongly enriched in metallic Pd.

2. EXPERIMENTAL

Samples of amorphous $PdZr_2$ alloy were studied as 9 mm × 13 mm × 0.05 mm foils mechanically fixed to a variable temperature sample holder. Activation turned the foil into a very brittle state.

The instrument used consists of a horizontal transfer system which allowed manipulation of the sample at variable temperatures ranging from 77 to 900 K. The stainless steel system was passivated for the reaction investigated by annealing the empty carrier in 300 mBar CO for 48 h at 770 K which caused a carbon overlayer to form on all hot parts of the system. The preparation chamber can be used as a flow through reactor with ca. 2.5 L volume. Mass flow controllers and a differentially pumped quadrupole mass spectrometer allow controlling and monitoring of catalytic performance. Reactions can also be carried out at low pressures and monitored *in situ* by a second quadrupole mass spectrometer. The base pressure of the chamber was 1×10^{-9} mBar. The sample can be transferred through a gate valve sealed and differentially pumped transfer chamber into the main analysis chamber in which surface analysis is performed at a base pressure of 1×10^{-10} mbar with the sample loaded. Differential pumping of the transfer system along its way ensures a minimum of contamination which was checked by repeated surface analysis as a function of transfer time. The experiments described here were done at a transfer time of 60 s, in which time the sample was removed from atmospheric pressure and surface analysis had started.

The analysis chamber is equipped with a Leybold EA 11 energy analyser and sources for XPS (Mg k α, 1253.6 eV, 90 W power, analysis with pass energy 50 eV) UPS (He I 21.22 eV, He II 40.8 eV, analysis with pass energies of 2 eV and 20 eV, respectively) and AES (5 keV, 100 nA sample current, 2 × 3 mm^2 sample raster, analysis with retarding ratio 4 and numerical differentiation with 2 eV modulation). A sputter gun was used for reference experiments. The energy

scale was calibrated to Au $4f\frac{7}{2}$ 84.0 eV. A ring electrode mounted near the entrance slit of the analyzer allowed exposure of the sample surface to a homogeneous electrostatic field of variable strength and polarity. With this device it is possible to detect surface differential charging which is likely to occur at inhomogeneous surfaces (*7*).

Gases were of highest available purity (99.997%), dried over molecular sieves and applied through stainless steel piping. The conditions of activation and reaction testing are given in Section 3.

Scanning electron microscopy was performed with a JEOL JSM 40 instrument at 25 keV acceleration voltage. The highest possible performance of the instrument was obtained with a narrow aperature and very low beam currents. Specimens were mounted on graphite blocks using colloidal graphite paint. Images of the precursor material were also obtained on a JEOL CX 200 TEMSCAN instrument with 200 keV acceleration voltage. Specimens were mounted on the graphite holder using a double-tilt side-entry stage. Both instruments were equipped with EDX facilities which allowed verification that all structures contained both elements Zr and Pd. No indication of macroscopic segregation was observed with any of the samples studied. The specimen pretreatment is described in Section 3.5.

3. RESULTS

3.1. Surface Composition

3.1.1. Qualitative analysis. The qualitative surface composition of the metallic glass samples was checked at various stages of treatment by Auger electron spectroscopy. These data are dominated by an intense O KLL feature. Other relevant element signals are displayed in Fig. 1 representing a section of derivative Auger spectra. Besides the expected elements Zr and Pd all samples contain Ar which was incorporated during the melt spinning process. In the crystallized sample significant amounts of sulfur and potassium were segregated at the surface from the bulk following the high temperature treatment. This treatment seems to "mix up" the surface components with the bulk alloy as can be seen from the loss of the intense nitrogen signal. It arises from zirconium nitride (see Section 3.2.2) which is also present on the activated

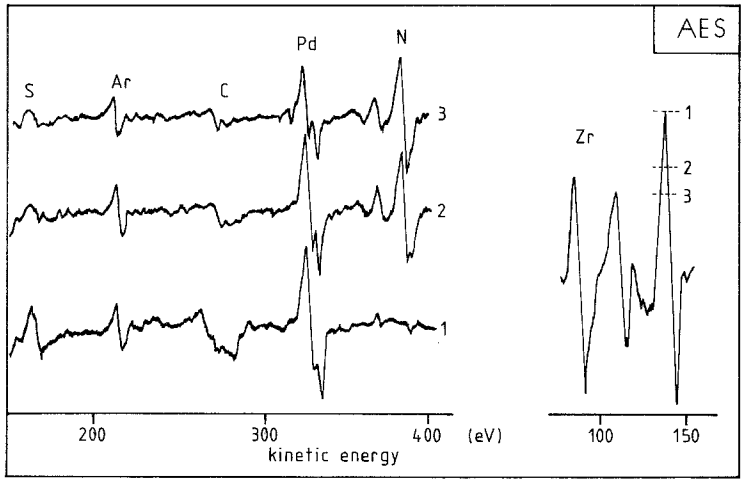

FIG. 1. Sections from the Auger spectra of $PdZr_2$ catalyst materials. Sample designations: 1 = UHV crystallised, 2 = *in-situ* activated, 3 = precursor. The dashed lines in the Zr spectrum denote the peak heights in the respective states of the surfaces. The wide Auger peak for carbon overlaps with the potassium peak.

TABLE 1

Surface Composition of $Pd_{33}Zr_{67}$ Alloys

Element in at%	As prepared	Activated[a]	Crystallized
Pd	4.5	4	7
Zr	17	31	38
O	32	55	32
C	45	10	21
K	1.5	0.1	2
Ratio Pd : Zr	0.26	0.13	0.19
D–Pd–XPS	14	12	21
D–Pd–CO	n.d.	5.9	n.d.

[a] After 15.7 h on stream at 553 K.

surface and which is far too stable to be decomposed in a heat treatment up to 773 K. The activation process increases the surface abundance of Pd which is little affected by the UHV crystallization process.

3.1.2. Quantitative XPS analysis. High-resolution XPS data were quantified by subtracting a stepped background, integrating and cross-section correction using Scofield's (*8*) parameters. The Pd 3*d* core level region strongly overlaps with the Zr 3*p* core levels: a scaled contribution for Zr determined independently from the Zr 3*d* data was subtracted from the total integral of the Pd + Zr region. The use of the Pd 3*p* core levels for quantification is not possible due to the overlap of Pd $3p\ \frac{3}{2}$ with O 1*s* (which was also corrected in a similar way as described above) and the weakness of the Pd $3p\ \frac{1}{2}$ line for the small abundancies occurring here. The corrected results are summarized in Table 1.

The surface composition deviates in all cases significantly from the bulk composition as no sputter cleaning was applied. The gas–solid interfaces are characterized by segregation of Zr to an extent depending on sample treatment. As can be seen from the Pd : Zr ratios the untreated surface represents best the bulk composition (Pd : Zr ratio 0.49 for nominal composition). The segregation of the reactive metal Zr is in line with the presence of high abundancies of oxygen. The carbon contamination is high on the strongly polar oxide surface of the untreated sample and is drastically reduced after catalysis despite of the fact that the reaction feed contains a carbon source. The nonmetal impurities S, Ar, and N amount with weak signals to less than 5% in the samples and were not included in the quantification. The only significant metal impurity was K, the surface abundance of which on the activated sample is, however, near the detection limit of XPS. The reduction in surface abundance may be caused by the formation of agglomerates of potassium carbonate as thermal desorption is not likely to have occurred.

The abundance of the active component Pd is low as a consequence of the pronounced segregation of Zr/O. This is reflected in the dispersion number given in the table which is here defined as the XPS abundance relative to the bulk abundance. Activation enhances this dispersion by a factor of 3 and as a consequence of the "mix up" in the UHV crystallization process the surface of the crystallized sample reflects even better the bulk composition. The dispersion from XPS of the activated sample can be compared to the dispersion determined by CO chemisorption which is, with 5.9%, half as large. Taking into account the different levels of information depth of the two methods it can be concluded that the Pd surface is neither porous nor composed of large spherical particles. Both morphologies would give rise to large differences in dispersion numbers between the truly surface sensitive chemical method and the spectroscopic determination. The observed values are a valuable indicator for the presence of platelets of Pd as seen in the HTEM (*2*) being a typical surface feature.

3.2. Thermal Crystallization of the Amorphous Precursor

This process was studied as reference experiment since it was found that such samples are far inferior in catalytic conversion than *in-situ* activated materials(*1, 2*).

3.2.1. UPS results. Figure 2 shows two typical He I (21.22 eV) spectra of a metallic

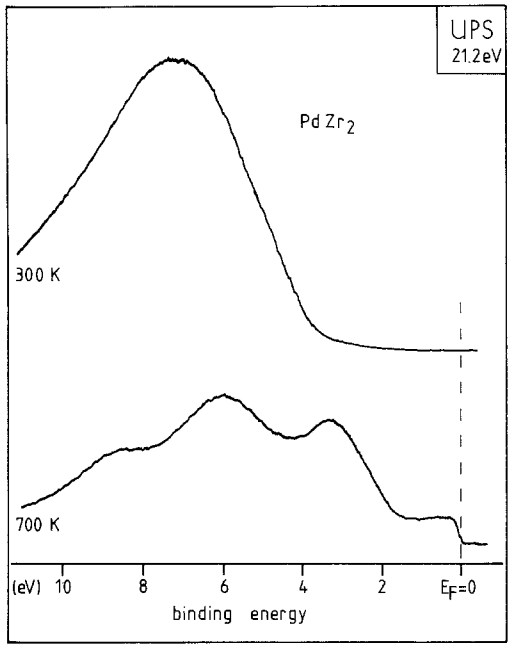

FIG. 2. He I UPS data for the precursor (top) and the UHV crystallized sample (bottom). Both spectra were recorded at 300 K.

glass sample before and after crystallization by heat treatment in UHV. The drastic change occurs at 700 K, spectra at intermediate temperatures are very similar to the initial spectrum. The surface of the precursor is an insulator (no density of states near the Fermi energy) with the peak at ca. 7 eV arising from oxygen $2p$ states indicating the presence of an oxide overlayer which is fully in line with the quantitative results. This surface is also the starting interface for the *in-situ* activation which occurs below 700 K and hence can not begin with chemisorption on metallic sites (e.g., Pd particles).

At 700 K suddenly a Fermi edge feature appears and the surface becomes metallic. Three peaks at 3.4, 6.2, and at 8.6 eV arising from molecular orbitals appear. In corresponding He II (40.8 eV) spectra a dominating peak at 6.3 eV occurs with smaller structures located at 8.3 and at 11.2 eV. None of these peaks is associated with the valence band spectrum of the bulk alloy which is known to consist of two peaks of similar intensity in a distance of 4.0 eV. One of them arising from Zr $3d$ states contains the Fermi edge, whereas the high energy structure arises from Pd $4d$ states (*9*).

The shape of the spectrum near the Fermi edge does not allow the conclusion that metallic palladium (the noble metal in the alloy) is present at the surface. The spectrum rather points to a heterogeneous surface made up from Zr metal particles embedded in a matrix of Zr compounds such as oxides carbides or nitrides. This also follows from the quantitative data which indicate the presence of 91 at% Zr, oxygen and carbon. The peak at 3.5 eV is likely to arise from Zr carbide the spectrum of which is characterised by a small Fermi edge and a dominant peak at 3.5 eV extending to about 7 eV (*10*). The structure at 6.2 eV is due to oxygen $2p$ states characteristic of many metal oxides. The structures at 8.3 and 11.2 eV point to the presence of chemisorbed water (*11*).

In summary vacuum crystallization of the alloy leads to a metallic heterogeneous solid consisting of Zr metal and Zr compounds. No positive indication for the presence of Pd at the surface was found.

3.2.2. XPS results. Having established that at 700 K the sample is metallic, chemical shifts in XPS can be used to identify the nature and relative abundance of the Zr compounds and to locate the palladium.

In Fig. 3, high-resolution spectra are displayed of the Zr $3p$ and Pd $3d$ region. The Pd $3d$ peaks are identified as sharp lines superimposed on the wide Zr $3p$ spectra. The main transformation of the solid occurs at 700 K as seen in UPS. At 650 K there is only very little change compared to the 300 K spectrum, and at 773 K the spectrum is similar to the 700 K data with only the amount of low energy peaks in the Zr subspectra being larger than at 700 K. Further heating to 900 K does not lead to any change.

The Pd is clearly present as oxide with a binding energy (b.e.) of 336.6 eV for the $3d\frac{5}{2}$ main transition (*5*). The $3d\frac{3}{2}$ peak is located in the gap between the Zr peaks and allows

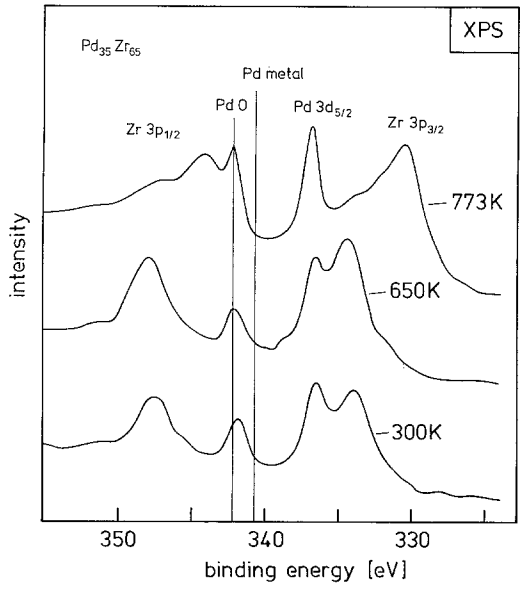

FIG. 3. XPS data from the Pd $3d$ + $3p$ region. The sample is *in-situ* UHV crystallized with the temperatures giving the measuring temperatures. Data acquisition time for each spectrum was 6 h. No metallic Pd can be detected.

thus to exclude that some metallic Pd is present.

Zr is present in several compounds and changes its chemical environment profoundly with heating: at 773 K a significant low energy shift indicates the formation of some metal in agreement with the UPS data. A more detailed analysis is done with the Zr $3d$ data.

The persistence of the Pd oxide against heating is unexpected, in particular in the presence of strongly reducing Zr metal. Pure PdO is completely converted to the metal at 773 K with a characteristic b.e. of 335.3 eV (*4, 5*). No indication of metal formation is seen, however, with the PdO particles in the crystallised sample. The thermal stability of the Pd oxide may be explained within the catalyst model proposed in Part I of this work(*2*): the large interface between Pd oxide and a shell of Zr oxide allows efficient exchange of oxide anions between the two oxides and thus prevents the formation of Pd metal nuclei necessary for the thermal decomposition reaction. The Zr oxide shell further inhibits the direct contact between Zr metal and Pd oxide which would be essential for a solid-state reduction process.

High resolution Zr $3d$ spectra obtained during *in-situ* UHV crystallization are displayed in Fig. 4. The data show intense features above ca. 180 eV and weak peaks below 178 eV which are due to X-ray satellites which were not removed in this set of data. The structure at 179.6 eV is superimposed on a satellite structure which was removed in data shown in Section 3.3.2.

At 300 K the amorphous metal is covered by a layer of zirconium oxide which is thin enough to allow the detection of a small signal of Zr metal (peak at 179.6 eV) from the bulk material. The low thickness of the oxide layer, the occurence of only one sharp C $1s$ contamination signal and the position of the corresponding O $1s$ signal at 531.6 eV (characteristic for hydroxyl) allow the conclusion that no charging interferes with the b.e. determination in XPS. As the oxide layer was charging in the more surface sensitive UPS experiment it can be concluded

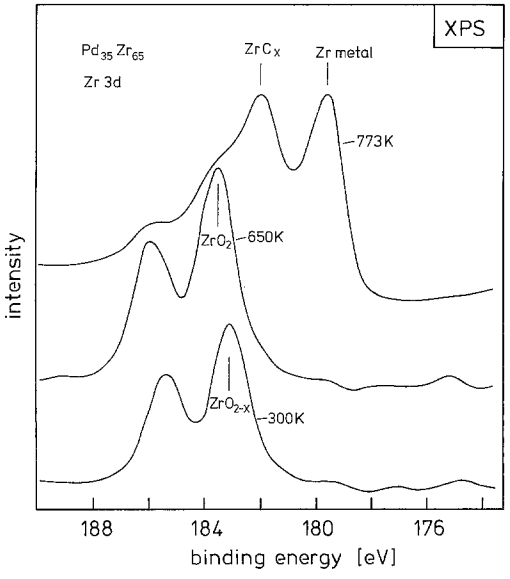

FIG. 4. XPS data from the Zr $3d$ region for the same experiment as shown in Fig. 3. The small peaks at low binding energy are due to X-ray satellites.

that the layer is thin and homogeneous at 300 K and not a holey film with islands of metal at the surface. The b.e. of 183.3 eV is significantly lower than observed for Zr dioxide for which 184.7 eV has been found in a similar overlayer on Ni–Zr alloys (*12*). Taking into account the simultaneous presence of N, C, and O (see Auger data) it can be concluded that the overlayer is not a binary compound but a mixture of ternary oxocarbides (C 1*s* b.e. 282.2 eV with about 70 at% of the carbon being present as a carbon–oxygen contamination, e.g. carbonate, with a b.e. of 287.2 eV) and oxonitrides (N 1*s* b.e. 397.4 eV). This complex nature is indicated by the subscript "*x*" in Fig. 4.

Thermal treatment to 650 K seems to cause some annealing of the complex overlayer as can be seen by the slight b.e. shift. The increase in signal intensity is due to a loss of the carbon oxygen contamination. The metal contribution has now disappeared indicating a growth of the layer thickness.

At 700 K a drastic change in the surface composition started which was completed at 773 K. The data at this stage are dominated by an intense doublet feature with Zr $3d\frac{5}{2}$ b.e. of 179.8 eV, characteristic of metallic Zr. The overlayer material is, however, still present as can be seen from the shoulders at the positions of the main lines of the spectrum at 650 K. An additional peak overlapping with Zr $3d\frac{3}{2}$ transition from the metal is assigned to Zr carbide with the corresponding C 1*s* peak at 282.8 eV contributing to ca. 80% of the total carbon abundance.

Most of the Zr compounds in the initial overlayer of the metallic glass are extremely high-temperature resistant. It is thus concluded that crystallization has caused a mechanical rupture of the overlayer followed by a segregation of crystallized Zr metal. Within this matrix the still oxidic palladium particles with their shells of Zr compounds are embedded as well as those components of the previous overlayer which are not soluble in Zr metal.

In summary, the surface of UHV-crystallized amorphous Pd Zr_2 deviates quite drastically from the homogeneous bulk composition found in XRD. It is made from elemental Zr with a large number of "slag" particles dispersed. Some of these oxygen-containing materials form a shell around particles of Pd oxide which are formed from the Pd metal component. These Pd oxide particles remain stable at 773 K due to the protective action of the Zr "slag."

From this analysis it is obvious that such a surface will have very little initial catalytic activity as the Pd is not metallic. After possible reduction of the Pd oxide particles by the reaction gas, a phase separation of the noble metal Pd from the "slag" will occur leading to free Pd metal particles supported on Zr oxides not dissimilar to conventional supported catalysts as they were prepared in this work (*2*) as reference material. This precrystallized catalyst will thus remain of inferior catalytic performance compared to the *in-situ* crystallized material which is expected to exhibit a different surface chemistry than described in the previous section.

3.3. The Surface of the in-Situ Activated Material

First attempts to analyse the highly active catalysts after transfer from the test reactor in air led to the detection of only oxidic materials which were perfectly stable against heat treatment at the level of the catalyst operation temperatures. This result was independent of the previous catalytic performance of the samples which led to the conclusion that the character of these surfaces was caused by the transfer procedure and that the real active surface is not air stable. Exposure of the amorphous precursor to the reaction gas mixture at pressures up to 10^{-3} mBar caused a change in the surface composition but did not lead to any catalytic activity. So it proved essential to activate the catalyst under atmospheric pressure in a reaction chamber, to characterize the surface by its catalytic activity and then to perform the surface analysis. Once a sample had been activated at atmo-

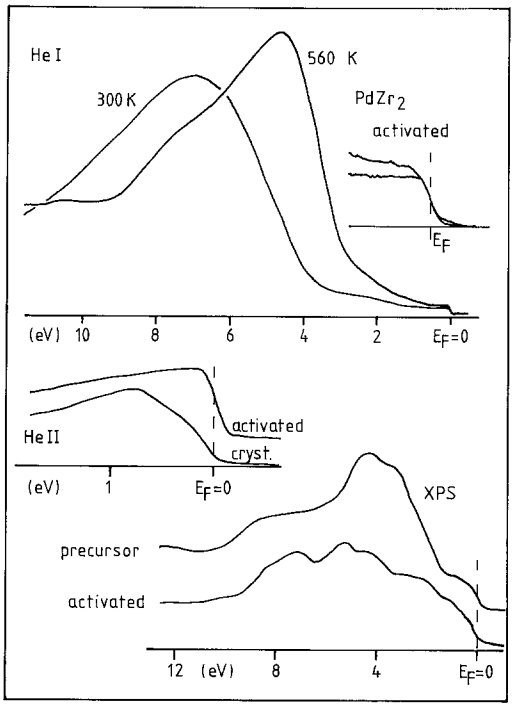

FIG. 5. Valence band data for the catalyst before and after activation in the high-pressure attachment. The valence band spectra are shown for different excitation energies (He I = 21.22 eV, He II = 40.8 eV, and XPS = 1253.6 eV). The spectral resolution is better than 0.1 eV for UPS and 0.8 eV for the XPS data.

spheric pressure, it showed also catalytic activity under reduced pressure. This allowed determination of the quality of the surface after the frequent sample transfers into the UHV and gave an opportunity to perform some real *in-situ* monitoring of the reaction.

3.3.1. UPS results. The conditions of activation and transfer required considerable fine tuning until reproducible spectra were obtained. Care was taken to approximate the activation conditions to those used in the catalytic testing procedures described in Part I of this work (*2*). The final conditions of activation were: a differential flow through reactor with a gas feed of 10 ml/min of a mixture containing each 1700 ppm O_2/CO in nitrogen. Temperature was raised to 560 K within 60 min under flowing Ar and then the reaction gas mixture was applied. After 16 h on stream the sample was cooled at 10^{-8} mBar to 450 K and transferred into the analysis chamber. Spectral data were recorded at 450, 560, 665, and 300 K, representing characteristic temperatures for transfer, catalyst operation, onset of crystallization, and possible low-temperature segregation.

In Fig. 5 typical He I data are collected and compared to XPS valence band data. The spectra of the hot activated surfaces are distinctly different from those of the UHV crystallized sample (see Fig. 2). The active surface is characterized by a small metallic contribution (Fermi edge), a peak at 2.4 eV, a dominant structure at 4.6 eV, and small features at 7.6 eV and 10.4 eV. All these features can be ascribed to molecular orbital peaks from oxygen species, namely of chemisorbed oxygen (2.4 eV), lattice oxygen (4.7 eV) (*5, 7*) and from hydroxyl groups (*13*).

Cooling the sample to 300 K does not affect the surface species giving rise to the Fermi edge feature but transforms the main component into an insulating form characterized by the same featureless secondary electron spectrum as observed with the as-prepared sample (see Fig. 2).

No molecular CO characterized by two peaks at 8.3 and 11.3 eV (*14*) can be detected either in the spectra seen in Fig. 5 or in corresponding He II data. As it is known from the chemical dispersion measurements that the surface chemisorbs CO at least at 300 K, the sample was dosed with CO at 300 and 450 K. In both cases it required 20,000 Langmuir exposures to observe the expected CO pattern. This is unusual for Pd as substrate the clean surface of which can be saturated with CO at 300 K after several Langmuirs of exposure (*14*). These experiments show, however, that some Pd must be present at the surface since CO is only dissociatively chemisorbed on Zr metal (*11*). The Pd causes also the Fermi edge feature which is supported by the shape of this feature in the He II spectrum which is

displayed in Fig. 5. The triangular shape is typical for Pd (*5, 7, 14*) whereas the reference spectrum with the low density of states is typical for the spectrum of metallic Zr (*11*) (see also XPS data in Fig. 4). The insensitivity of the Pd against contamination (in the cool down experiment) and the very low sticking probability for CO both point to a special form of Pd which will be related to a solid solution of oxygen in Pd.

The XPS valence band data shown also in Fig. 5 allow verification of the assignments of the UPS data and analysis of the samples in a less surface-sensitive way than by UPS (1250 eV kinetic energy of the emitted electrons corresponds to a ca. 10-fold larger depth of information than for 20 eV "UPS" electrons). The metallic character of both samples can be seen by the onset of the spectra at 0 eV representing the Fermi edge with ca. 20 times worse resolution than in UPS. For the precursor sample this is an indication that the oxide layer which rendered it insulating for UPS is significantly thinner than the information depth of valence band XPS.

Broad features at 1.4, 4.5, 5.3, and 7.7 eV can be seen with different relative intensities in both spectra. The relative cross sections for the elements O : C : Pd : Zr are 1 : 0.1; 200 : 25, which allows assignment of oxygen 2*p* and/or Zr 4*d* states to the peaks. The structures close to the Fermi level arise from metallic Zr 4*d* states; the prominent feature at 4.5 eV in the precursor is ascribed to hybridized states between Zr 4*d* and carbon or oxygen 2*p* states. Such a structure has been found in the valence-band spectrum of Zr carbide of unknown purity (*10*). The intensity above 5 eV is due to oxygen 2*p* emission from oxide anions.

In summary, the valence-band information allows the conclusion that in the activated catalyst a fraction of metallic Pd is present, dispersed into a matrix of oxide material. Under working conditions this oxide exhibits a certain conductivity which is lost after cooling the surface to 300 K. The XPS valence-band spectrum indicates the presence of a significant amount of metallic material also in deeper layers and confirms (as concluded from AES and UPS data) that during activation a thin Zr oxide overlayer is removed from the catalyst. The existence of this overlayer is associated with the induction of the catalytic activation described in Part I of this work (*2*). The CO chemisorption properties of the Pd particles are different from those of the pure element.

3.3.2. XPS data. The core-level data can again be interpreted in terms of chemical shifts as the valence band information has ascertained that no electrostatic charging is to be expected. A possible surface differential charging which is characteristic of heterogeneous nonmetallic surfaces was excluded in the following way. An electrostatic field was applied between sample and electron analyzer and spectra were recorded with zero field and differently polarized electrostatic fields on. The spectra were shifted in an exactly symmetric way relative to the zero-field spectrum which excludes the operation of a surface-inherent electrostatic field and thus differential charging (*7*).

Figure 6 shows data of the Zr 3*p* and Pd 3*d* region for two experiments in which a precursor was activated in the reaction mix and in pure CO respectively (in this data set only the Pd $3d\,\frac{5}{2}$ and Zr $3p\,\frac{3}{2}$ peaks are displayed). Clear shifts of the Pd core levels to lower b.e. are associated with the activation process. This is different from the UHV crystallization experiment (see Fig. 3) where no shift occurred. The b.e. shifts from 337.6 eV (Pd $3d\,\frac{5}{2}$) and 342.9 eV (Pd $3d\,\frac{3}{2}$) for 1.5 eV to 336.0 eV and 341.5 eV for the practical activation. In the model experiment the shift of 2.2 eV is even larger and leads to a b.e. of 335.4 eV for Pd $3d\,\frac{5}{2}$. Only this b.e. is typical for metallic Pd which is found at 335.5–335.0 eV (*3, 4, 5, 7*). After the practical activation the Pd $3d\,\frac{5}{2}$ line with a shift of 1.4 eV is significantly wider and more asymmetric as typical for elemental Pd (FWHM given by the natural linewidth of the photon source, ca. 0.95 eV) (*5, 15*). Finally it is pointed out that in pure CO a

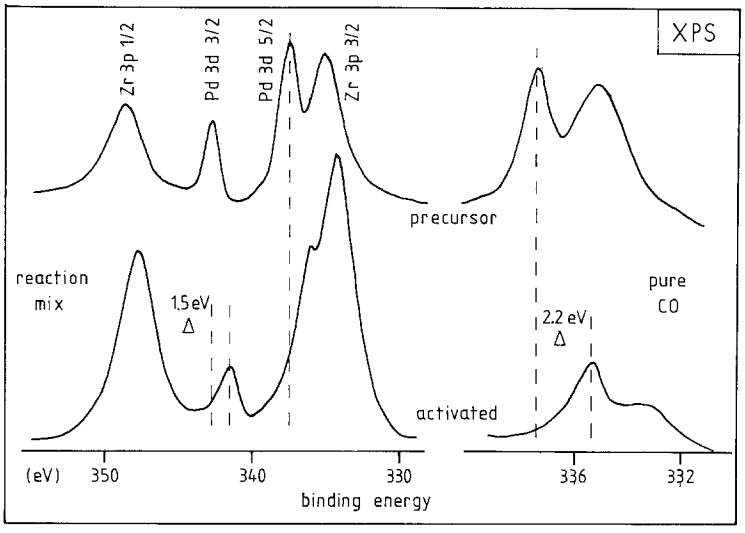

FIG. 6. XPS data of the Pd 3*d* and Zr 3*p* regions for the catalyst before and after activation in the high-pressure attachment. Activation gases were the reaction mixture (1700 ppm O_2 and CO) and 1700 ppm CO, respectively. Both gases were diluted in nitrogen. Activation temperature was 560 K. The spectra are X-ray satellite subtracted.

massive segregation of Pd takes place being finally more abundant than Zr; the inverse effect occurs in reaction atmosphere (see Table 1, ratio Pd : Zr).

After activation in reaction atmosphere the surface Pd is thus converted into an intermediate form between metal and oxide; in the presence of pure CO pure metallic Pd is present at the surface. The intermediate state of the active Pd characterised by its chemical relative stability and its "chemical" shift of the Pd 3*d* $\frac{5}{2}$ line of 0.7 eV is ascribed to the presence of oxygen dissolved in the Pd lattice (*16*). Such a solid solution compound was described as resulting from thermal decomposition of PdO and the spectroscopic parameters of this compound are well compatible with the present observations (*4*, *5*). A widening of the Pd metal lattice was indeed found in the XRD analysis of the activated catalysts described in Part I of this work (*2*).

The wide Pd line in the spectrum of the active surface is an indication that several Pd species are present. The line is as wide as in the case of the oxidic particles embedded in a metallic matrix (1.4 eV FWHM of Pd 3*d* $\frac{5}{2}$) which was obtained after crystallization (compare Fig. 3). The active Pd particle is thus characterized by a gradient of the oxygen abundance which is in all volume elements of finite size allowing a core of oxide to co-exist with a shell of metal–oxygen solid solution.

These particles are embedded in a zirconia matrix. Characteristic spectra are displayed in Fig. 7. The Zr 3*d* spectra are satellite corrected and allow the assignment of small peaks. The low energy peak at 179.6 eV (dashed line) arises from the metallic bulk of the precursor sample. The main peak at 183.4 eV is characteristic of zirconia. Its b.e. is fairly variable between ca. 183 and 184 eV (*12*, *17*), indicating the structural and elemental nonstoichiometry of the material which has not been subjected to a high-temperature treatment. Different samples of the precursor alloy exhibit shifts of the zirconia line relative to the metal peak of ca. 0.5 eV.

After activation the b.e. is shifted significantly to lower b.e. and a peak at 182.4 eV seems to indicate the presence of a suboxide. Such compounds like Zr_3O do exist but are not stable in oxidizing conditions of the

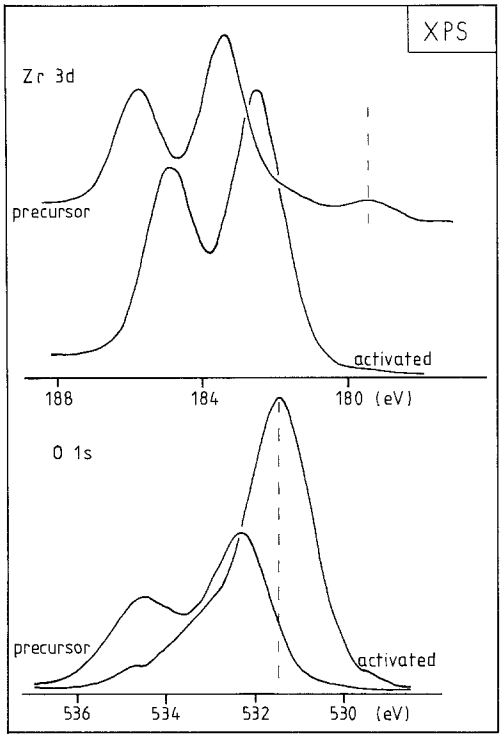

FIG. 7. XPS data of the Zr 3*d* region (top) and O 1*s* region (bottom) for the activation experiment in the reaction mixture shown in Fig. 6. The spectra are satellite subtracted. The dashed line in the Zr 3*d* spectrum denotes the position of Zr metal, the line in the O 1*s* spectra the position for oxide O^{2-} ions in zirconia.

catalytic environment. The high b.e. of the corresponding oxide anions of 531.4 eV (see lower part of Fig. 7, dashed line) also points to the presence of strongly polarising Zr^{4+} ions. The shift of Zr 3*d* is thus likely to be caused by the transformation of an insulating water containing oxyhydroxide into a better defined ion conducting oxide present after activation. The oxygen 1*s* data of the precursor support this, as activation leads to a massive loss of the water (534.5 eV) and hydroxyl (532.3 eV) species. The contribution to the oxygen 1*s* peak of the activated surface at 533 eV is due to the presence of chemisorbed oxygen (*18*). All oxygen b.e. are ca. 1.0 eV higher than found with typical other oxides (*19*) due to the strong intra- and extra-atomic deshielding effects of the highly charged Zr^{4+} ion.

The detection of nonstoichiometric zirconia is characterized by a change in the b.e. distance O 1*s*–Zr 3*d* 349.0 after activation.

The chemical nature of the potassium impurity was studied in detail as it is well known that potassium is a promotor in many catalytic reactions and can act as an agent increasing the sticking probability of a difficult to adsorb species (*20*). The abundance of potassium on the activated surface is much smaller than on the initial surface or after crystallization. It occurs on these surfaces as an ionic species with a K $2p\,\frac{3}{2}$ b.e. of 293.5 eV typical, e.g., KOH. After activation the b.e. shifts to 295.0 eV, which is 1 eV higher than the highest known b.e. for potassium compounds. As differential charging was excluded this can only indicate that potassium is incorporated into the zirconia. The high b.e. follows from the extra-atomic screening of the Zr^{4+} ion for the particularly sensitive K^+ ion (*21*). The dissolution into the oxide layer also explains the loss in surface abundance as thermal desorption under the given conditions is unlikely. The whole effect may be of importance for the catalytic operation as doping of a potential ion conductor (zirconia) with alkali ions may enhance the ion conductivity significantly.

In summary, the simultaneous presence of a reducing component and an oxidising component in the reaction gas atmosphere lead to a different surface chemistry of the catalyst than after thermal treatment in UHV or pure CO or O_2. The active surface contains metallic Pd as an oxygen loaded solid solution and a oxygen deficient Zr oxide with no Zr metal present.

3.4. In-Situ Reaction Profiles

After the detection of chemisorbed surface oxygen and the Pd + O solid solution, reaction experiments were performed to assess the catalytic relevance of these findings. The experiments were done in a small UHV chamber equipped with a quadrupole mass spectrometer, gas inlets for oxygen, CO and reaction mixture and a pumping sys-

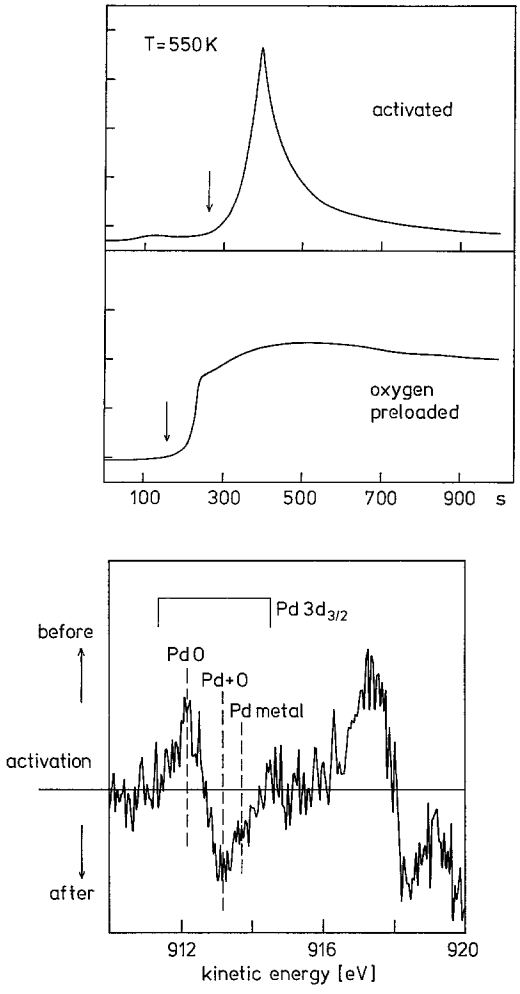

FIG. 8. Top: traces of *in-situ* reaction experiments with an activated catalyst. The intensity of the mass 44 signal for CO_2 is recorded vs time. The arrows denote the admission of CO (see text). Bottom: XPS difference spectrum of the Pd 3*d* region, the spectrum after activation of the sample used in the top experiments was subtracted from the spectrum of the precursor.

tem allowing treatments at atmospheric pressure (for activation) and at 5×10^{-8} mBar base pressure. This chamber was placed between the high pressure cell and the surface-analysis chamber. This arrangement allowed the activation of a sample under practical conditions (flow reactor), to characterize the surface and then to carry out "*in situ*" reaction experiments.

The significant results are summarized in Fig. 8. In the top panel the response curves at *m/e* 44 of treated catalysts to a pulse of pure CO admitted for 10 s $\times$ 10^{-3} mBar are shown at the time indicated by the arrow. In the top experiment the sample was activated in the flow reactor for 4 h, transferred at 400 K and the base pressure, and finally heated to 550 K for 10 min in the base vacuum, which slightly degraded due to the loss of some molecular oxygen and water.

The response does not begin with the admission of the CO but only after a time which is much longer than the thermal equilibration time (ca. pulse duration). The fact that oxidization occurs at all indicates that the catalyst has a storage function for the oxidant. The location is most likely not the top surface (chemisorbed oxygen) but the subsurface region. From there it requires a short time of migration until the oxidant is available for the chemical reaction. The storage capacity for either CO or oxygen is rather limited as can be seen from the abrupt loss of CO_2 partial pressure with time.

In a second type of experiment the catalyst was preloaded with oxygen by an exposure of 60 sec to 10 mBar of O_2 at 300 K. After this pretreatment of an activated catalyst an almost continuous response to the same CO pulse as applied in the first experiments was obtained as can be seen from the respective trace in Fig. 8. This indicates that the shape of the first response was due to depletion of oxygen in the surface—near region of the catalyst volume. It is a special property of the catalyst material to be able to store oxygen under comparatively mild conditions which ensures the existence of the partly reduced metal components in the system. It is pointed out that this property was also tested under real catalytic operation conditions where shut off of the oxygen supply allowed the reaction to continue over 20 min (*2*).

The amount of stored oxygen after exposure to pure oxygen increases rapidly with raising temperature above 300 K until at a certain critical temperature below 500 K total oxidation of the catalyst surface occurs

(loss of the Pd metal features in XPS). These experiments show that the catalyst has the ability to form and to store chemically reactive oxygen independent of its immediate use in oxidation.

As a result of this chemically active oxygen the Pd in the CO/O_2 atmosphere is not activated to pure metal but to a solid solution of oxygen in metal which can be seen in XPS difference spectra (bottom panel of Fig. 8) measured before and after the experiments described above. The relatively short duration of the activation (4h) did not lead to a significant enrichment of Pd. The difference spectrum is thus obtained from equally large peaks and reflects the shifts of the peaks. The positions of the Pd $3d\frac{3}{2}$ peak for different chemical states of Pd are indicated by dashed lines. It is apparent that the Pd is reduced after activation from the oxidic state into the solid-solution state.

3.5. Internal Microstructure of the Alloy

In the course of this investigation it was found that the catalyst should consist of small particles with anisotropic shape. Such a microstructure is unusual for a metallic material. The surface morphology changes upon activation from a smooth structure into a layer of agglomerates stretching over the base alloy. The size of the agglomerates containing Zr and Pd was found to be ca. 100 nm. UHV crystallization seems to cause a reshaping of the surface in which the initial oxide layer is mechanically removed like a slag material.

An attempt was made to image the internal microstructure of the catalyst by chemical etching and scanning electron microscopy and to compare it to the surface morphology. Such information can help to understand the usefulness of a rapidly quenched material as catalyst precursor.

Samples of amorphous and UHV crystallized alloy were etched in a special way which preserved the crystal structure of the material as was checked by XRD. An electrochemical cell with the sample and a platinum electrode was constructed with 0.1 M NaCl as electrolyte. The cell was loaded with 1 MΩ external resistance and a very gentle corrosion was observed within 24 h. Chemical analysis of the electrolyte by AAS ensured stoichiometric dissolution of less than 10 wt% of the samples. The washed surfaces were subjected to high resolution SEM investigations.

Figure 9 shows the internal structure of a UHV crystallized sample. Sharp contours of steps are characteristic of well-developed platelet crystals. The individual crystals have large dimensions in the layer plane and exhibit thicknesses below 100 nm.

The etched precursor shows a completely different internal microstructure as can be seen in Fig. 10. The inset is a view onto the untreated outer surface which appeared to be completely smooth in the images shown in Part I. The entire microstructure is made from stacks of irregular smooth shaped platelets with dimensions of ca. 50 to 250 nm in the layer plane and ca. 10 nm thickness. The contours of the platelets were made visible by modifying the analog SEM contrast with its derivative.

The etched precursor sample was activated in the same way as described above and showed after 16 h on stream the same activity as catalysts prepared from non-etched precursors. After 24 h on stream the sample was transferred to the microscope and images as shown in Fig. 11 were obtained. The sample has developed a grain structure in the μm size (cracks in Fig. 11). Each grain exhibits a terraced surface with irregular step contours. Superimposed are agglomerates of platelets with a rough surface. Such platelets are likely to be the objects studied by HRTEM in Part I of this work. The rough surface is due to the microcrystalline internal structure of each platelet giving rise to the large interface area between zirconia and palladium. This image shows an early stage of the process leading to the final catalyst structure with the dense layer of agglomerates seen in the SEM micrographs in Part I.

In summary these images clearly show

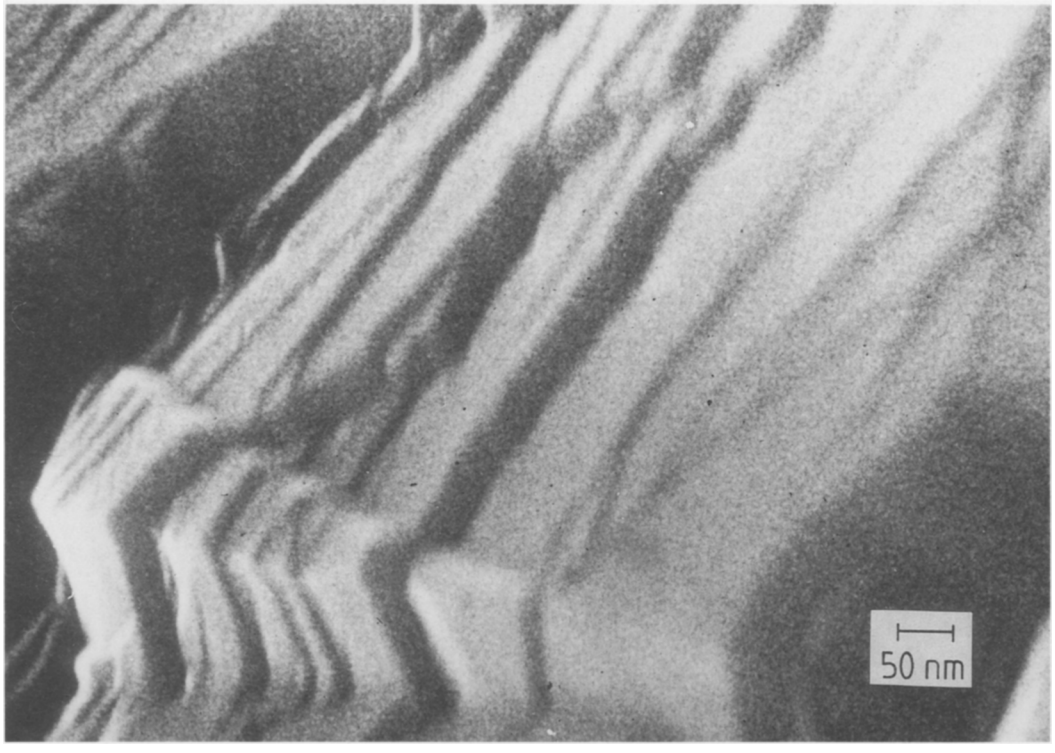

FIG. 9. High-resolution SEM image of Pd Zr_2 after UHV crystallization and etching of the surface.

that the catalyst exhibits a microstructure made from small platelets throughout the bulk of the material. In the activated form these platelets form irregular aggregates whereas the circular shape of the platelets is lost after UHV crystallization. They grow into large regularly-shaped crystalline sheets. The irregular platelets exhibit a fine internal structure and represent the active form of the catalyst. The analysis of this form has been described earlier and is fully in line with the conclusions from the spectroscopic surface analysis.

4. DISCUSSION

The surface of amorphous $PdZr_2$ alloys including their natural contaminations has been modified by a heat treatment in various atmospheres. The resulting surfaces were different for different exposures and in all cases very different from the bulk compositions detected by powder XRD. The surface reactions are controlled by the partial pressure of oxidizing agent in the atmosphere. All reactions start from an interface of a thin but dense poorly defined zirconia (containing also nitrides and carbides) and PdO adlayer over a bulk of amorphous alloy. The zirconia further contains some water and holds an overlayer of chemisorbed water which is not lost at 300 K in UHV.

At low partial pressures of oxidizing agent (annealing in UHV) heat treatment to the catalyst operation temperature causes an improvement of the definition of the oxide layer. Heating to 770 K leads to crystallization of the alloy, a process which breaks up mechanically the oxide layer and allows metallic Zr to appear on the surface. The release of mechanical strain associated with the formation of crystals from the amorphous precursor was clearly detected in SEM images of heat treated surfaces. Thermal decomposition of the oxide layer is very

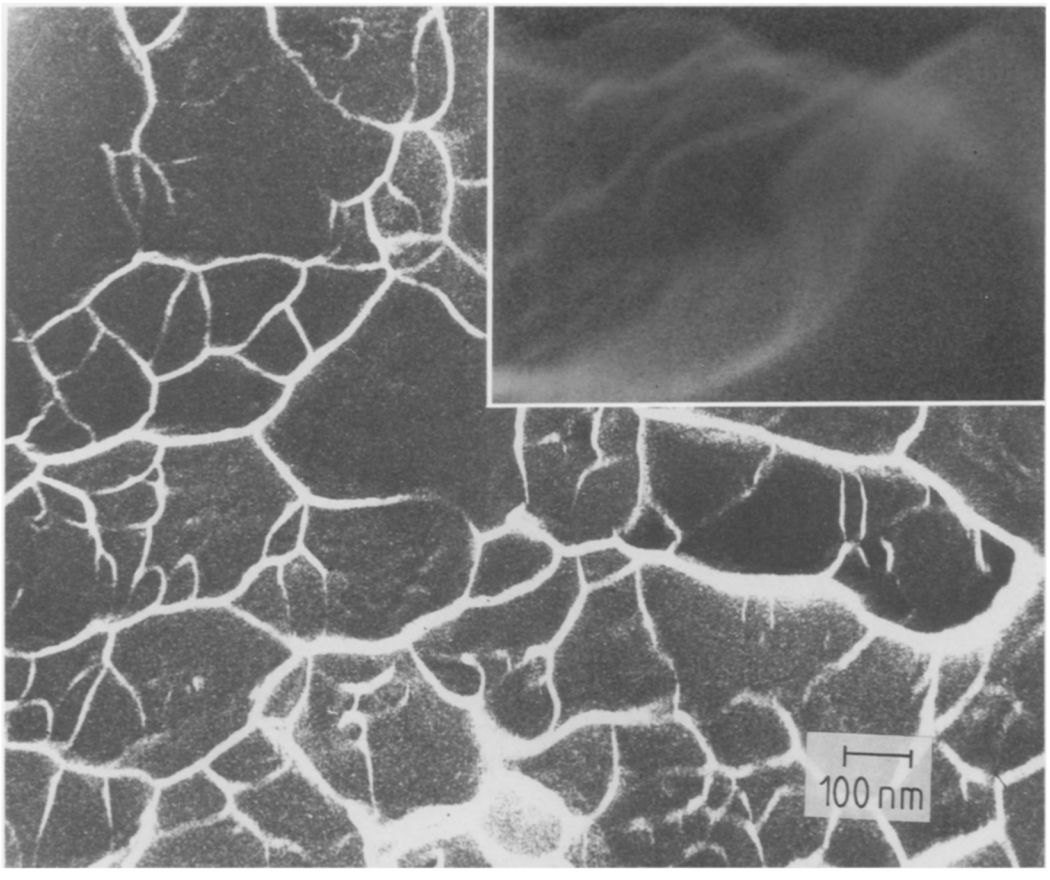

FIG. 10. SEM of the activated catalyst before (inset) and after etching of the surface. The inset image was obtained in the high-resolution mode of the JEOLCX 200 TEMSCAN instrument (see experimental). The step contrast in the main image was enhanced by adding the first derivative of the video signal to the primary signal.

unlikely at these moderate temperatures. The palladium oxide should, however, have been thermally decomposed at the crystallization temperature which is not observed. Neither thermal stress nor the presence of strongly reducing Zr metal reduce the Pd. This is a strong indication that the PdO particles are surrounded by a zirconia layer which does not only mechanically isolate the PdO from the Zr metal matrix but also supplies some oxygen to the PdO preventing the formation of metal nuclei and thus thermal degradation. This is in line with the observations in the HRTEM where irregular and extended interface areas were detected between palladium and zirconia species.

At high partial pressures of oxidizing agents (activation in pure oxygen, loading of preactivated catalysts with pure oxygen) the surface is covered with a thick layer of oxides of Zr and Pd. No traces of underlying or embedded metal can be detected. In this state the material is virtually catalytically inactive.

At high partial pressures of reducing agents (activation in pure CO) the surface becomes strongly enriched in metallic palladium which does not contain any dissolved oxygen. This state is unstable with respect to oxygen exposure leading to a drastic loss of Pd against growth of a Zr oxide phase.

The case of activation in reaction mixture

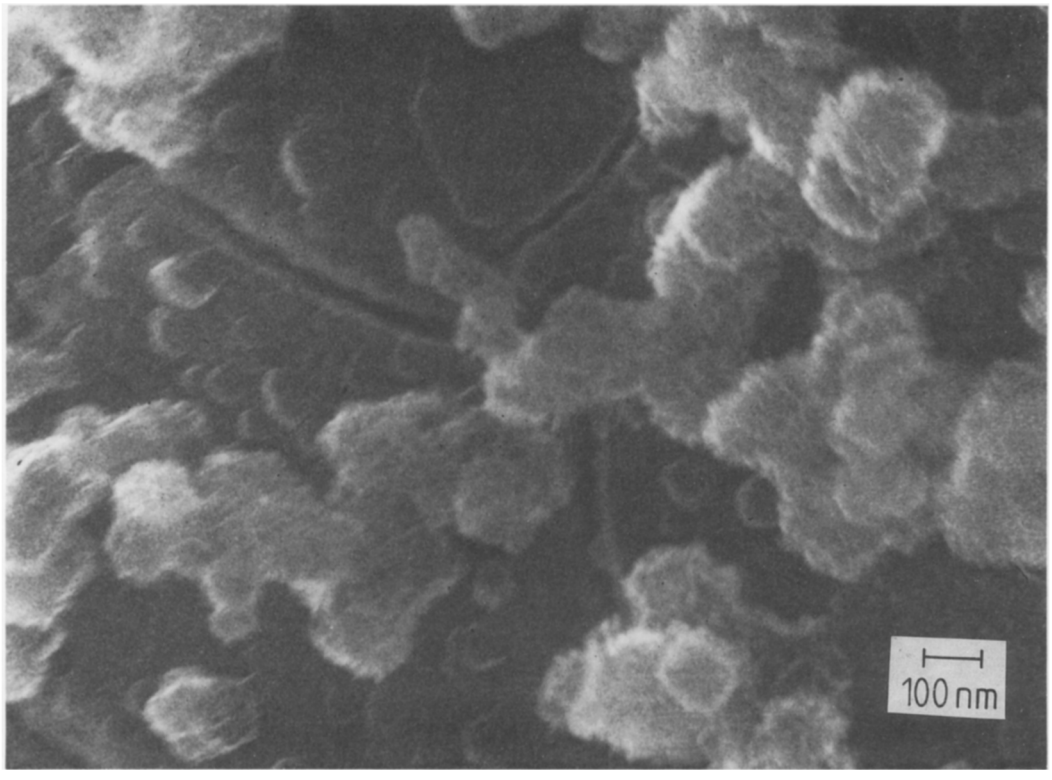

FIG. 11. SEM image of the sample from Fig. 10 after activation.

consisting of intermediate partial pressures of both reducing and oxidizing agents leads to a special and intermediate surface composition. A matrix of hydroxyl-free nonstoichiometric zirconium oxide contains particles of partly reduced palladium. These particles are made up from Pd metal containing dissolved oxygen and from residual oxidic Pd. These particles are large enough that a Fermi edge feature can be observed although the atomic abundance is only 4 at%. A possible thin overlayer of "spritted" Pd over zirconia can be excluded from the agreement of the XPS dispersion value with the CO titration of the exposed Pd surface. The existence of particles is further confirmed by XRD and HRTEM data presented in part one of this work.

Evidence was found that the zirconia may be doped with traces of potassium ions. These ions which occur as a bulk impurity of the alloy and which segregate at the surface during crystallization, forming there a fraction of a monolayer, are almost absent on the catalytically active surface. The unusually high b.e. of the weak potassium signal points to their presence within the zirconia where the high cation charge causes extra-atomic screening and so the high "chemical" shift.

The surface of the zirconia was covered with excess chemisorbed oxide ions after catalytic testing. This points to its role as oxygen supply medium for the catalytic reaction centers located at the palladium. From reaction experiments it is known that the activated catalyst can store significant amounts of oxygen. It is further well known that nonstoichiometric zirconia is a good ion conductor for oxide ions. This property of the activated form of zirconia is also indicated by the low b.e. of Zr 3*d* which at 182.4

eV is significantly lower than in previously measured zirconia phases (184.7 eV for stoichiometric and 183.0 eV for nonstoichiometric zirconia ex Ni–Zr amorphous alloys). The low value agrees with literature data (182.3 eV) for UHV annealed zirconia. The shift of the Zr 3*d* line from 183.4 eV in the ill-defined precursor overlayer to 182.4 eV in the activated phase does not reflect a change in the valence of the Zr, which is in both cases Zr^{4+}. The downshift indicates the improved screening of the cationic charge by the oxide anions with replacing hydroxyl groups or other atoms by oxygen, i.e., with increasing compositional and structural definition of the oxide which is also essential for the ion conductivity. In no case does the shift indicate a substantial deficiency of oxygen in the oxide causing the partial reduction to e.g. Zr^{3+} ions, as such compounds would be instable with respect to the presence of oxygen at elevated temperatures in the catalytic environment.

Within the zirconia matrix, accounting for ca. 80% of the total surface atoms, particles of palladium are dispersed. The chemical state of the Pd is intermediate between metal and oxide but is, e.g., characterized by Fermi edge feature. The existence of such an intermediate state of Pd has been discussed several times in the literature and was also recently suggested to be relevant in CO oxidation over Pd as concluded from non-spectroscopic arguments (*22*). The structure of oxygen-charged Pd is similar to that of the metal differing from it by the presence of oxygen atoms in the vacancies between the metal atoms. This filling of the vacancies (gap radius in Pd 554 pm, covalent radius of oxygen 620 pm) causes the lattice to expand slightly which gives rise to the enlarged *d*-spacings found in the XRD of activated catalysts (*2*). It is assumed that only a small fraction of the available gaps will be filled with oxygen which has to diffuse through defects in the solid. Aggregates of oxygen in defects ("bubbles") are not a good model for this compound as no lattice expansion and integral change in spectroscopic properties of Pd can be expected from a coarse distribution of the gas. The XPS parameters found for the catalyst in this work (precursor 337.5 eV, activated 336.0 eV, and segregated pure metal 335.3 eV) are in good agreement with recent literature data (*4, 5, 7*). The shift between pure metal and solid solution is mainly caused by a change in lineshape (*5*), which cannot be detected, however, in the spectra of the dilute Pd particles of the catalyst.

The following picture of the *activated surface* can be obtained from a combination of all results presented here. The surface is strongly enriched in zirconium oxide giving rise to a Pd : Zr ratio of 0.13 versus 0.5 for the bulk. It is contaminated with carbon atoms which do not form a carbide. It is also likely to be doped with an impurity of potassium. The zirconia contains only one type of Zr^{4+} ions and allows the definition of a Fermi energy in the gap of the insulator. The corresponding anion spectrum shows the presence of a large majority of oxide ions and a small amount of a second species which is attributed to chemisorbed molecular oxygen. The eventual presence of hydroxyl impurities cannot be ruled out.

Essential for the defined electronic properties of the zirconia matrix is the presence of a finely divided Pd species which is metallic conducting. Valence band spectra and the comparison of surface abundancies obtained by spectroscopy and CO chemisorption indicate that these Pd particles form indeed part of the outer gas–solid interface and are not encapsulated in the zirconia matrix. The interface between the two phases is large enough that the Fermi energies of the two phases defined by the metallic properties of the Pd + O phase and the defect concentration in the zirconia can equilibrate resulting in a common work function for both components. The density of states at the Fermi energy remains unaffected by changes in the sample temperature which cause a modification of the oxygen species present at the surface. Clean Pd shows a drastic change in the *d*-band intensity after

adsorption of small amounts of oxygen (*23*). This insensitivity of Pd against oxygen is unusual and attributed to the "contamination" of the metal with oxygen.

The catalyst can store significant amounts of oxygen which are located not only in the subsurface region of the Pd particles (easily accessible for oxidation) but also in the bulk of the matrix, from where it can diffuse to local concentration minima located in the Pd particles after the oxidation reaction has depleted the subsurface oxygen there. Under the conditions of the model reaction experiments it is the filling of the catalyst with oxygen which determines the reaction rate.

The catalyst properties depend on the intimate contact of the two functional constituents the Pd particles as reaction centers and the zirconia as storage and transport medium for oxide ions. This contact is achieved by a maximum interface area resulting from a disc shape of the particles. This unusual morphology is the direct consequence of the manufacture of the precursor with the melt-spinning technique. It leads to flattened droplets forming layers in the bulk of the starting material. Activation at moderate temperatures in the presence of both reducing and oxidizing agents leads to crystallization of the material in the droplets. UHV crystallization or chemical induced segregation of either Pd (in reducing conditions) or Zr (in oxidizing conditions) destroys the droplets and leads to large regular but still anisotropic crystals. Such materials are of little catalytic value as they have lost the large interface between the constituents. This large interface can also not be generated by conventional preparation of the catalyst from a zirconia support with wet impregnation.

It has not been shown in this work that the unusual state of the Pd as solid solution with oxygen is intrinsically better suited for CO oxidation than pure Pd in the same morphology. Under the catalytic conditions used in this work it seems that the abundance of chemisorbed oxygen is important for the overall performance. The novel catalyst from a melt spinning prepared precursor offers the possibility to maximize the abundance of oxygen at the reaction centers.

The activated catalyst is still a metastable state on the way to a mixture of large crystals of Pd and zirconia. Fluctuations in the relative partial pressures of the gas feed or in temperature may trigger the transformation of the metastable active form into the stable form, which is expected to show similar catalytic performance as the conventional impregnated catalyst. A most useful catalyst is thus prepared from a homogeneous amorphous precursor with minimum temperatures of activation and operation.

ACKNOWLEDGMENTS

We thank M. Rebholz for experimental help with reference experiments to the Pd + O system. This work was financially supported in part by DEGUSSA AG, LONZA AG, and by the Fonds der Chemischen Industrie.

REFERENCES

1. Baiker, A., Gasser, D., and Lenzer, J., *J. Chem. Soc. Chem. Commun.* 1750 (1987).
2. Baiker, A., Gasser, D., Lenzer, J., Reller, A., and Schlögl, R., *J.Catal.* **126,** 555 (1990).
3. Legare, P., Hilaire, L., Marie, G., Krill, G., and Amamou, A., *Surf. Sci.* **107,** 533 (1981).
4. Peuckert, M., *J. Phys. Chem.* **89,** 2481 (1985).
5. Noack, K., Zbinden, H., and Schlögl, R., *Catal. Lett.* **4,** 145 (1990).
6. Nowotny, J., and Sloma, M., *in* "Surface and Near Surface Chemistry of Oxides" (J. Nowotny and L. C. Dufour, Eds.), p. 310 ff, Elsevier, Amsterdam, 1985.
7. Paal, Z., Loose, G., Weinberg, G., Rebholz, M., and Schlögl, R., *Catal. Lett.* **66,** 301 (1990).
8. Scofield, J. H., *J. Electron Spectrosc.* **8,** 129 (1976).
9. Oelhafen, P., Hauser, E., Güntherodt, H. J., and Bennemann, K. H., *Phys. Rev. Lett.* **43,** 1134 (1979).
10. Jhara, H., Mirahayaski, M., and Nakagawa, N., *Phys. Rev.* **13,14,** 1707 (1976).
11. Zehringer, R., Hauert, B., Oelhafen, P., and Güntherodt, H. J., *Surf. Sci.* **215,** 501 (1989).
12. Armbruster, E., Baiker, A., Güntherodt, H. J., Schlögl, R., and Walz, B., *Stud. Surf. Sci. Catal.* **31,** 389 (1987).
13. Barteau, M. A., and Madix, R.J., *Surf. Sci.* **146,** 108 (1984).
14. Conrad, H., Ertl, G., Küppers, J., and Latta, E. E., *Faraday Discuss. Chem. Soc.* **58,** 116 (1974).

15. Schlögl, R., Noack, K., Zbinden, H., and Reller, A., *Helv. Chim. Acta* **70,** 627 (1987).

16. Matushima, T., and White, J. M., *Surf. Sci.* **67,** 122 (1977).

17. Wiemhöfer, H. D., Harke, S., and Vohrer, U., *Solid State Ionics* **40,** 433 (1990).

18. Henrich, V. E., *Prog. Surf. Sci.***9,**143 (1979).

19. Briggs, D., and Seak, M.P., "Practical Surface Analysis," p. 599. Wiley, New York, 1990.

20. Schlögl, R., *in* "Alkali Metals in Heterogeneous Catalysis in Physics and Chemistry of Alkali Metal Adsorption" (H. P. Bonzel, G. Ertl, and A. M. Bradshaw, Eds.), p. 347, 1989.

21. Muhler, M., Schlögl, R., and Ertl, G., *J. Catal.*, in press.

22. Ladas, S., Imbihl, R., and Ertl, G., *Surf. Sci.* **219,** 88 (1989).

23. Conrad, A., Ertl, G., Küppers, J., and Latta, E. E., *Surf. Sci.* **65,** 245 (1977).